UNIVERSITY OF NIS FACULTY OF MECHANICAL ENGINEERING

THE TENTH INTERNATIONAL CONFERENCE
TRANSPORT AND LOGISTICS
https://doi.org/10.46793/TIL2025.225T

til 2025

FEM-BASED ANALYSIS OF DELAMINATION EFFECTS ON THE BALLISTIC LIMIT OF A COMPOSITE PLATE

Jovica TASIĆ[1], Dragan MARINKOVIĆ[2]

[1)]Department of Transport Engineering and Logistics, Faculty of Mechanical Engineering, University of Niš, Serbia
[2)]Department of Structural Analysis, Institute of Mechanics, Berlin Institute of Technology, Germany,
Department of Transport Engineering and Logistics, Faculty of Mechanical Engineering, University of Niš, Serbia

ORCID iDs: Jovica TASIĆ https://orcid.org/0009-0009-9860-8631
Dragan MARINKOVIĆ https://orcid.org/0000-0002-3583-9434

Abstract

This paper presents a numerical investigation of the ballistic limit of a composite plate under projectile impact using finite element (FE) simulation. The response is modeled through a dynamic explicit analysis to capture the highly transient behavior within a short time interval. The composite plate, designed using high-impact-resistant Kevlar 49 with a ±45° ply orientation, is configured to enable monitoring of interlaminar delamination during penetration. A 9 mm caliber projectile is modeled at varying velocities, incrementally increased until the penetration threshold is identified. This approach enables a systematic evaluation of the ballistic resistance of the composite plate against the selected ammunition. The primary advantage of the method lies in its non-destructive nature, avoiding the material loss and costs typically associated with experimental testing.

***Keywords**: finite element analysis, high-velocity impact, numerical simulation, composite plate, ballistic limit, delamination.*

1 INTRODUCTION

Composite materials are characterized by high strength combined with low specific weight, making them a suitable choice for enhancing the performance of existing solutions, modifying finished products, or developing new prototypes. Huang et al. [1] demonstrated the use of composite materials for structural reinforcement and improved resistance. Their analysis revealed opportunities for optimization in terms of robustness, weight reduction, material consumption, and production cost. Schmid et al. [2] performed optimization of composite material parameters on a CAD (Computer-Aided Design) model. Accordingly, the application of composites remains extensive and a subject of active research aimed at achieving more efficient utilization. Some prominent fields of application include the automotive industry [3], transportation [4], aerospace engineering [5], medical applications [6], and civil engineering [7]. A particularly important role is observed in the defense industry [8], where composites provide both structural and ballistic protection [9, 10]. Motivated by these favorable characteristics, an analysis of composite materials was conducted. Given the wide range of existing composites, this study was preceded by a review of current solutions [11, 12]. Based on their properties, composites were classified and selected according to matrix material, reinforcement type, reinforcement geometry and continuity, manufacturing process, intended application, and other criteria. The focus of this work is on multilayer laminates reinforced with unidirectional continuous fibers. By comparing different materials, Kevlar 49/epoxy was selected due to its favorable impact resistance. Previous studies [13] confirmed the ballistic performance of Kevlar 49-based composite plates under projectile impact. Its current use in protective applications further supports its selection, as numerous ballistic vests, helmets, and armored vehicle components are already manufactured using this material [14–17]. This study examines the ballistic resistance of the proposed armor plate against a 9 mm projectile. The initial projectile velocity is varied within limits determined by the firearm characteristics, while the plate model consists of multilayer laminates with adhesive layers between each ply. In the event of complete penetration, the corresponding velocity is considered the ballistic resistance limit. Contribution of this work lies in the proposed procedure for efficiently determining the ballistic protection threshold under realistic conditions without destroying the specimen.

2 THEORETICAL BACKGROUND

The theoretical formulations applied to describe the impactor model and the composite plate are presented. Given that the impactor is metallic, it is modeled with the Johnson–Cook plasticity and damage formulations [18]. For the damage characterization of the composite laminates, the Hashin failure criterion [19] is employed, while interlaminar delamination [20] is represented using a traction–separation law.

2.1. Johnson-Cook Plasticity

The Johnson–Cook plasticity model is one of the most widely used constitutive formulations for predicting the behavior of ductile materials under conditions of large strains, high strain rates, and elevated temperatures. The model assumes that the flow stress can be expressed as a multiplicative combination of three contributions: strain hardening, strain-rate sensitivity, and thermal softening. The equivalent flow stress is defined according to Eq. (1) as:

$$\sigma = (A + B(\varepsilon)^n)\left[1 + C\ln\left(\frac{\dot{\varepsilon}}{\dot{\varepsilon}_0}\right)\right](1 - \hat{T}^m) \qquad (1)$$

where$A$ is initial yield stress, B hardening modulus, n strain-hardening exponent, Cstrain-rate sensitivity coefficient, $m$thermal softening exponent, εequivalent plastic strain, $\dot{\varepsilon}$ plastic strain rate, $\dot{\varepsilon}_0$ reference strain rate.The nondimensionaltemperature $\hat{T}$, which varies between zero and one (0 = room temperature, 1 = melting temperature), is defined according to Eq. (2):

$$\hat{T} \equiv \begin{cases} 0 & \text{for} \quad T < T_{transition} \\ \frac{(T - T_{transition})}{(T_{melt} - T_{transition})} & \text{for} \quad T_{transition} \leq T \leq T_{melt} \\ 1 & \text{for} \quad T > T_{melt} \end{cases} \quad (2)$$

In addition, the Johnson–Cook damage model is defined through the failure strain given in Eq. (3):

$$\varepsilon_f = \left[d_1 + d_2 e^{(d_3 \sigma^*)}\right]\left[1 + d_4 \ln\left(\frac{\dot{\varepsilon}}{\dot{\varepsilon}_0}\right)\right]\left(1 + d_5 \hat{T}\right) \quad (3)$$

whered_1-$d_5$are damage parameters andσ^* is the ratio of hydrostatic (volumetric) stress to equivalent shear stress.

2.2. Hashin failure criteria

Failure criteria in composite materials are used to predict damage under complex stress states. Due to their anisotropic nature, composites require criteria that distinguish between fiber and matrix failures, such as tension and compression modes. Failure criteria are presented using the notion of failure index. The failure indexis defined as the ratio of the applied stress to the material strength:

$$I_F = \frac{stress}{strength} \quad (4)$$

Failure is predicted when the failure index reaches or exceeds unity $I_F \geq 1$.

The Hashin failure criteria (HFC) are widely used to predict damage in composite laminates by distinguishing between fiber- and matrix-dominated failure modes. The model defines separate conditions for fiber tension, fiber compression, matrix tension, and matrix compression, allowing for a more accurate representation of composite behavior under multi-axial loading.The failure index is defined separately for each failure mode according to the following equations:

- Fiber tension mode:

$$I_{Fft}^2 = \left(\frac{\sigma_1}{F_{1t}}\right)^2 + \alpha\left(\frac{\sigma_6}{F_6}\right)^2 \text{ if} \sigma_1 \geq 0 \quad (5)$$

- Fiber compression mode:

$$I_{Ffc}^2 = \left(\frac{\sigma_1}{F_{1c}}\right)^2 \text{ if} \sigma_1 < 0 \quad (6)$$

- Matrix tension mode:

$$I_{Fmt}^2 = \left(\frac{\sigma_2}{F_{2t}}\right)^2 + \left(\frac{\sigma_6}{F_6}\right)^2 \text{ if} \sigma_2 \geq 0 \quad (7)$$

- Matrix compression mode:

$$I_{Fmc}^2 = \left(\frac{\sigma_2}{2F_4}\right)^2 + \left[\left(\frac{F_{2c}}{2F_4}\right)^2 - 1\right]\frac{\sigma_2}{F_{2c}} + \left(\frac{\sigma_6}{F_6}\right)^2 \text{ if} \sigma_2 < 0 \quad (8)$$

Where α is a weight factor to give more or less emphasis to the influence of shear on fiber failure.

In the above equations:

- F_{1t} denotes the longitudinal tensile strength,
- F_{1c} denotes the longitudinal compressive strength,
- F_{2t} denotes the transverse tensile strength,
- F_{2c} denotes the transverse compressive strength,
- F_4 denotes the transverse shear strength,
- F_6 denotes the longitudinal shear strength,
- σ_1, σ_2, andσ_6 are components of the effective stress tensor, σ, that is used to evaluate the initation criteria and which is computed from:

$$\sigma = \boldsymbol{M\sigma} \quad (9)$$

where **σ**is the true stress and ***M*** is the demage operator:

$$M = \begin{bmatrix} \frac{1}{(1-d_f)} & 0 & 0 \\ 0 & \frac{1}{(1-d_m)} & 0 \\ 0 & 0 & \frac{1}{(1-d_s)} \end{bmatrix} \quad (10)$$

whered_f, d_m, and d_s are internal (demage) variables that characterize fiber, matrix, and shear damage, which are derived from damage variables d^t_f, d^c_f, d^t_m, and d^c_m, corresponding to the four modes previously discussed, as follows:

$$d_f = \begin{cases} d_f^t \text{ if} \sigma_1 \geq 0 \\ d_f^c \text{ if} \sigma_1 < 0 \end{cases} \quad (11)$$

$$d_m = \begin{cases} d_m^t \text{ if} \sigma_2 \geq 0 \\ d_m^c \text{ if} \sigma_2 < 0 \end{cases} \quad (12)$$

$$d_s = 1 - \left(1 - d_f^t\right)\left(1 - d_f^c\right)\left(1 - d_m^t\right)\left(1 - d_m^c\right) \quad (13)$$

Fracture energy, defined as the area under the stress–strain curve from damage initiation to complete material degradation, provides a quantitative measure of the material's resistance to crack propagation after failure has begun, as shown in the Figure 1.

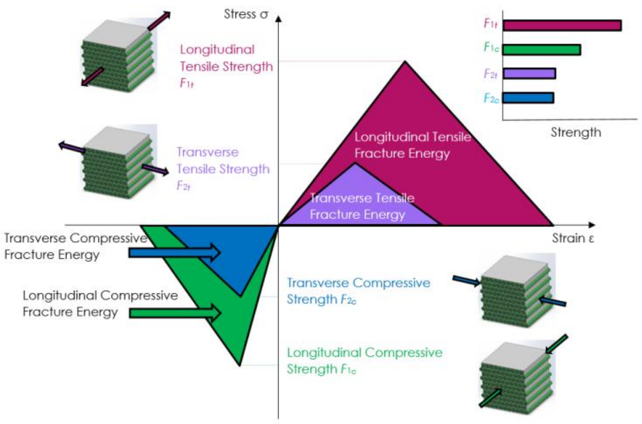

***Fig. 1** Fracture enegy of composite material*

By identifying the initiation of each failure mode, Hashin criteria support reliable analysis and design of composite structures.

2.3. Delamination

Delamination refers to the damage mechanism associated with crack formation between adjacent composite plies (inter-ply failure mode). Such degradation may develop under dynamic loading conditions, as in the present case involving impact. This phenomenon can be evaluated using a cohesive damage model in conjunction with fracture mechanics. The constitutive response of the interlayer material is illustrated in Figure 2. The separation between opposing surfaces is denoted byδ_i, while the corresponding interfacial stiffnessK_i, often referred to as the penalty stiffness, characterizes the elastic behavior prior to damage initiation.

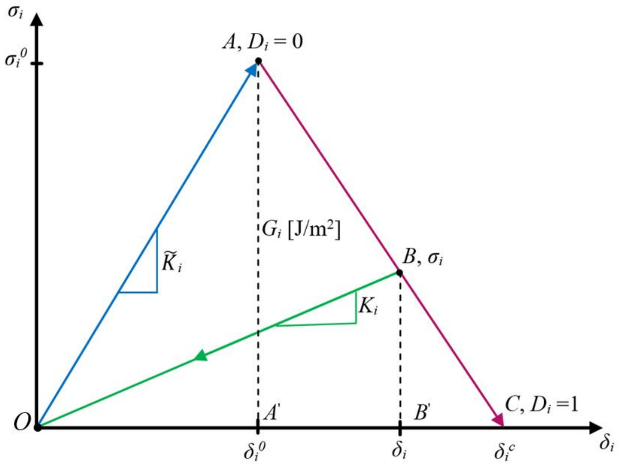

Fig. 2*Stress transfer in the cohesive zone model (CZM)*

The traction–separation relationship can be defined byEq. (14):

$$\sigma_i = K_i \delta_i \tag{14}$$

Here,$\sigma_i$denotes the traction, while $\delta_i$represents the separation between the opposing surfaces, with the interfacial stiffness$K_i$defined byEq. (15):

$$K_i = (1 - D_i)\widetilde{K_i} \tag{15}$$

where$D_i$is the damage variable and$\widetilde{K_i}$ [N/mm^3] is the stiffness of the undamaged interface. Damage initiation is governed by the condition $\sigma_i = \sigma_i^0$, whereas the critical separation is obtained from Eq. (16):

$$\delta_i^0 = \sigma_i^0 / \widetilde{K_i} \tag{16}$$

The evolution of the damage variable is defined as:

$$D_i = \begin{cases} 0, \ \delta_i \leq \delta_i^0 \\ 1, \ \delta_i = \delta_i^c \end{cases} \tag{17}$$

Based on the traction–separation diagram, once damage initiates the interfacial traction begins to decrease from its peak value σ_i^0. In the undamaged state ($D = 0$), the material retains its initial stiffness (segment *OA*). For $0 < D < 1$, the stiffness progressively degrades as damage evolves (segment *AC*). Complete failure occurs when D = 1, corresponding to point C on the curve.

Thus, four characteristic stages of material behavior are identified:

- Linear elastic response of the undamaged interface(*OA*)
- Onset of damage (*A*)
- Damage evolution and stiffness degradation (*AC*)
- Failure and crack formation (*C*).

3 FINITE ELEMENT ANALYSIS

The finite element method (FEM) was employed to accurately predict the structural response of the composite plate, with modeling and simulations conducted using the commercial software ABAQUS.The procedure for performing the finite element analysis (FEA) is presented in the following sections.

3.1. Geometry and FE mesh

As the study investigates the contact behavior between the impactor and the composite plate, their geometries were defined and translated into finite element models with mesh densities appropriate for accurate analysis.The impactor represents a 9 mm bullet grain and is modeled as an ellipsoidal shape with semi-axes of 10.5 mm and 4.5 mm, as illustrated in Figure 3.The impactor consists of two material regions: a lead core and an outer brass jacket with a uniform thickness of 1 mm.The total mass of the impactor is 8 g. For the numerical analysis, the impactor was modeled as a deformable body and discretized with 35,388 quadratic tetrahedral elements (C3D4).

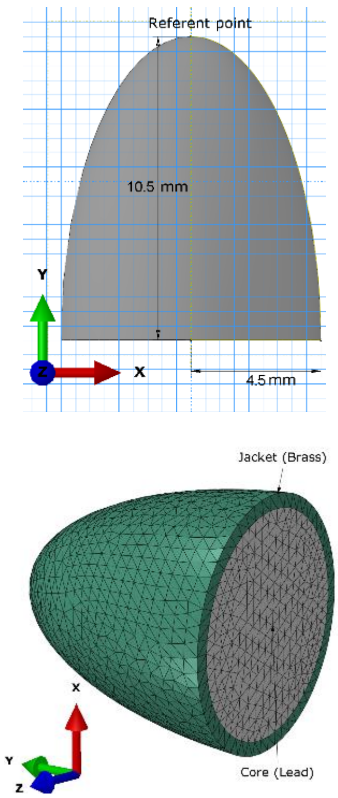

Fig. 3*Impactor model, bullet grain 9 mm and finite element discretization.*

The composite plate model exhibits a high level of complexity and is composed of several interconnected segments. The central region represents the interaction zone between the projectile and the plate and is described using a three-dimensional macro-scale model. Each composite laminate is modeled individually, along with the interlayer regions separating adjacent laminates. Their integration is achieved using a tie-constraint technique, resulting in a configuration consisting of ten laminates and nine interlayers. The composite layers are discretized with SC8R continuum shell elements based on works cited [21, 22] and assigned Hashin damage criteria. The interlayers are represented by COH3D8 cohesive elements governed by a traction–separation damage law, as illustrated in Figure 4.

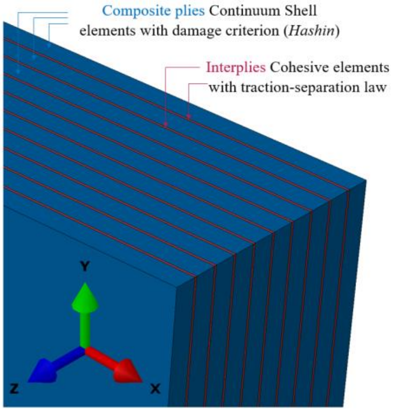

Fig. 4*Discrete and continuum damage models.*

The laminate orientation in the composite follows a[+45/-45]$_5$ stacking sequence relative to the referencex–axis, as shown in Figure 5. To enhance the accuracy of the numerical model, the mesh of each laminate was aligned with the fiber direction at an angle of 45°, as illustrated in Figure 5.

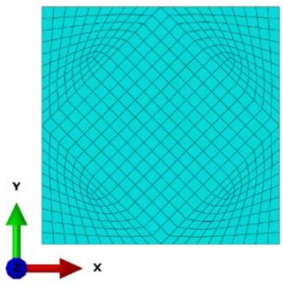

Fig. 5*Ply mesh discretization.*

Each laminate layer has a thickness of 0.5 mm, while the interlayer thickness is 0.05 mm, resulting in a total composite thickness of 5.45 mm. To reduce computational cost, the remaining portion of the composite plate is modeled at the meso-scale level (single-layer representation) using conventional S4R shell elements, also incorporating the Hashin damage criterion. These two modeling approaches are coupled through a solid-to-shell technique, forming a unified structural model.The composite plate measures 500 × 500 mm, with a central region of 30 × 30 mm represented by the detailed 3D model. The final mesh consists of 21,929 elements, and the complete model configuration is shown in Figure 6.

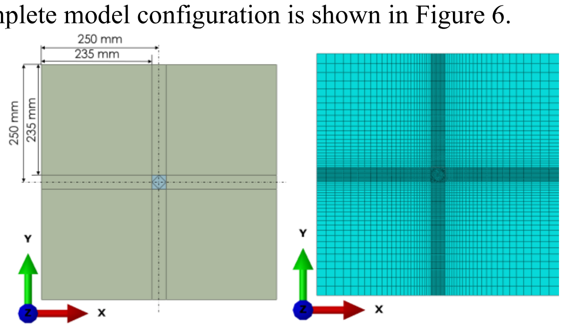

Fig. 6*Target model: composite platedimensions and FE discretization.*

3.2. Properties of Materials

Material properties were specified for both the impactor and the composite plate to accurately represent their mechanical behavior in the simulation. The impactor consists of two distinct materials: a brass jacket and a lead core. The mechanical behavior of these materials was defined using the Johnson–Cook constitutive model, with properties provided in Table 1.

Table 1 Material properties of the impactor

Property		Brass (jacket)	Lead (core)
Density, ρ	[kg/m^3]	8520	12000
Elastic modulus, E_1	[GPa]	110	210
Shear modulus, G	[GPa]	44	0.352
Poisson's ratio, υ		0.375	0.29
Yield strength, A	[GPa]	0.112	0.792
Hardening constant, B	[GPa]	0.505	0.51
Hardening coefficient, n		0.42	0,26
Strain rate sensitivity, C		0.009	0.014
Thermal softening coefficient, m		1.68	1.03
Melting temperature, T_m	[°C]	916	1520
Transition temperature, T_{tr}	[°C]	20	20
Initial failure strain, d_1		0.54	0.05
Exponential factor, d_2		4.89	3.44
Triaxiality factor, d_3		3.03	-2.12
Strain rate factor, d_4		0.014	0.002
Temperature factor, d_5		1.12	0.61
Reference strain rate		1	1

Based on the criterion that the material should be resistant to impact loads, a design for damage tolerance is recommended. As Kevlar fibers and tough matrices can provide the necessary impact and damage propagation resistance, the type of Kevlar 49 material was chosen.Kevlar 49/epoxy unidirectional composites are known for their high tensile strength, low density, and excellent energy-absorption capability. The aramid fibers provide strong resistance to stretching and tearing, while the epoxy matrix ensures effective load transfer and structural stability. These combined properties give the composite high impact resistance, allowing it to dissipate energy through mechanisms such as fiber deformation, matrix cracking, and controlled delamination.The material properties of the Kevlar 49/epoxy unidirectional composite, including density, elastic and shear moduli, Poisson's ratio, strength parameters, and fracture energy values, are summarized in Table 2.
For monitoring delamination, the material properties of the interlayer, expressed in terms of fracture energy in the normal and shear directions, are defined in Table 3.

Table 2 Properties of Kevlar 49/epoxy unidirectional material

Property		Value
Density, ρ	[kg/m^3]	1380
Longitudinal modulus, E_1	[GPa]	80
Transverse in-plane modulus, E_2	[GPa]	5.5
Transverse out-of-plane modulus, E_3	[GPa]	5.5
In-plane shear modulus, G_{12}	[GPa]	2.2
Out-of-plane shear modulus, G_{23}	[GPa]	1.8
Out-of-plane shear modulus, G_{13}	[GPa]	2.2
Major in-plane Poisson's ratio, υ_{12}		0.34
Out-of-plane Poisson's ratio, υ_{23}		0.40
Out-of-plane Poisson's ratio, υ_{13}		0.34
Longitudinal tensile strength, F_{1t}	[MPa]	1400
Transverse tensile strength, F_{2t}	[MPa]	30
Longitudinal compressive strength, F_{1c}	[MPa]	335
Transverse compressive strength, F_{2c}	[MPa]	158
In-plane shear strength, F_6	[MPa]	49
Longitudinal tensile fracture energy, G^L_{ft}	[J/m^2]	300
Longitudinal compressive fracture energy, G^L_{fc}	[J/m^2]	250
Transverse tensile fracture energy, G^L_{mt}	[J/m^2]	1000
Transverse compressive fracture energy, G^L_{mc}	[J/m^2]	1200

Table 3 Properties of interlayer damage model

Property		Value
Density, ρ	[kg/m^3]	1000
Normal stiffness, Knn	[N/m^3]	10^6
Shear stiffness, first direction, Kss	[N/m^3]	10^6
Shear stiffness, second direction, Ktt	[N/m^3]	10^6
Nominal stress limits, σ_n^0	[Mpa]	74.2
Nominal stress limits, first direction, σ_s^0	[Mpa]	110.4
Nominal stress limits, second direction, σ_t^0	[Mpa]	110.4
Normal mode, fracture energy, G_I	[J/m^2]	1000
Shear mode, fracture energy – first direction, G_{II}	[J/m^2]	2000
Shear mode, fracture energy – second direction, G_{III}	[J/m^2]	1800

3.3. Initial and boundary conditions

Initial conditions determine the movement of the bullet andthe boundary constraints of the plate.The bullet is defined to move in a straight line along the negative z-direction, with its velocity specified as a variable parameter.

The plate is fully supported along all edges by fixing all translational (U_1=U_2=U_3=0) and rotational (UR_1=UR_2=UR_3=0) degrees of freedom,as shown in Figure 7. The bullet impacts the central region of the plate at a right angle, generating the applied load. Since the maximum load occurs when the bullet strikes at 90°, this configuration represents the worst-case scenario for the plate.

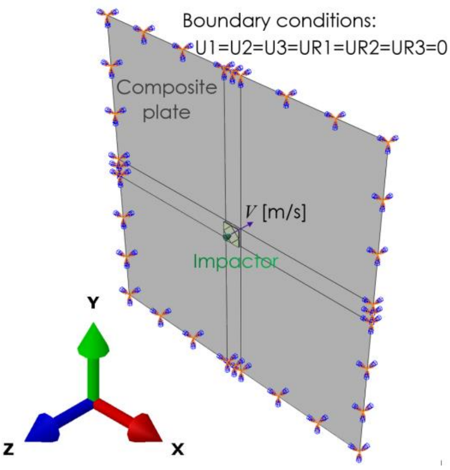

Fig. 7Initial position and boundary conditions

3.4. Simulation

The simulations were conducted using the prepared models of the projectile and composite plate in Abaqus. Explicit dynamic contact analyses were performed, accounting for the nonlinear impact behavior between the bullet andthe composite plate. An explicit solver with an automatic time increment was employed, with a total simulation period of t=2×10^{-4} s.The objective of this analysis is to evaluate the ballistic performance of the composite plate based on its ability to absorb the kinetic energy of the projectile. For this purpose, an algorithmic scheme was developed, as illustrated in Figure 8.

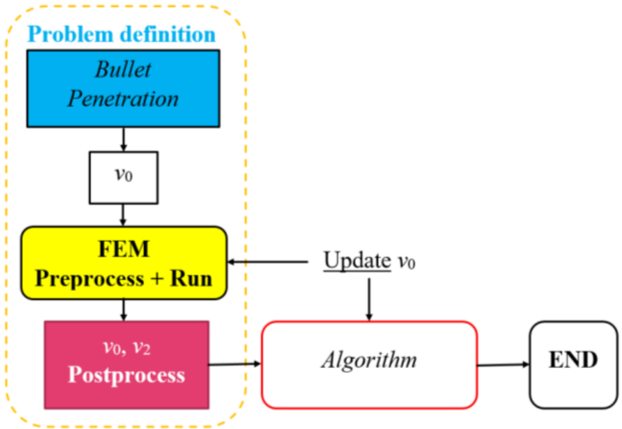

Fig. 8 *Algorithm for determining the ballistic limit of the composite plate*

According to the described algorithm, $v_0$represents the initial velocity of the projectile, while $v_2$denotes its velocity after impact. If v_2=0,the composite plate is capable of fully absorbing the projectile's kinetic energy at the given initial velocity v_0. Conversely, if 0<v_2<v_0, penetration of the projectile through the target has occurred. Upon completion of each simulation, the value of $v_0$is adjusted, and the cycle is repeated until the maximum velocity at which no penetration occurs is determined, within a specified tolerance for the velocity increment. This velocity defines the ballistic limit of the composite plate. The algorithm was implemented in Abaqus through the input file, with automation performed using Python scripts.

4 RESULT AND DISCUSSION

The simulation results were evaluated by monitoring the projectile's kinetic response, specifically the initial velocity $v_0$and the residual velocity$v_2$after impact. This comparison provides a clear indication of the composite plate's ability to absorb impact energy. Figure 9 shows the damage visualization for the case of projectile penetration at an initial velocity of 250 m/s. The left image illustrates fiber damage predicted using the Hashin fiber failure criterion, while the right image represents interlaminar damage, delamination between layers, expressed through the scalar damage variable. A value of this damage variable equal to one indicates that material failure has occurred.

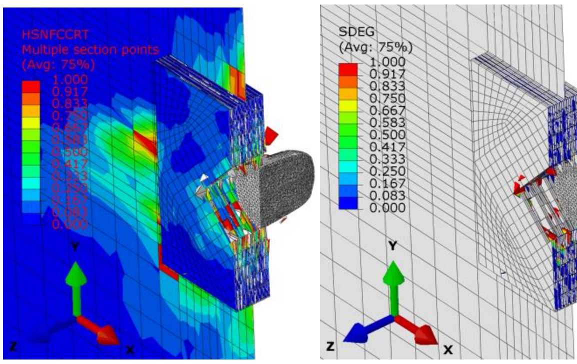

Fig. 9 *Projectile penetration with damage criteria*

Figure 10 presents the time history of the projectile's kinetic energy during the simulation. Based on the remaining kinetic energy of 9.64 J at the end of the impact event, the residual projectile velocity was calculated as v_2=49.1 m/s, according to Eq. (18). This value reflects the portion of energy not absorbed by the composite plate during penetration.

$$E_k = \frac{mv^2}{2} \rightarrow v = \sqrt{\frac{2E_k}{m}} \tag{18}$$

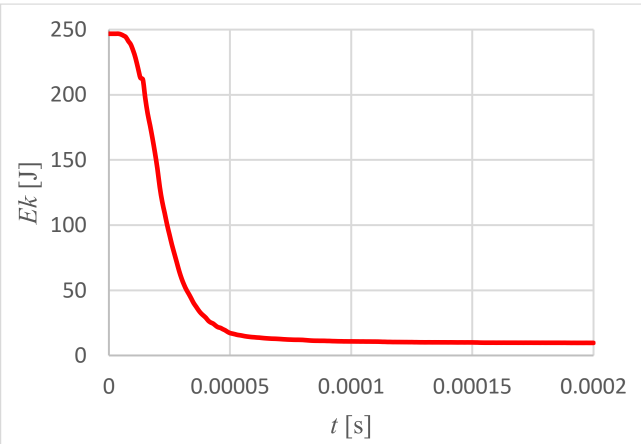

Fig. 10*Kinetic energy evolution of the projectile* *(v_0=250 m/s)*

Figure 11 illustrates the relationship between the initial and residual projectile velocities for all simulated impact scenarios. The maximum initial velocity considered was 550 m/s, consistent with the technical specifications of the projectile. From the presented results, the highest initial velocity $v_0$for which the residual velocityv_2=0 becomes zero is220 m/s. This value represents the ballistic limit of the composite plate, indicating the maximum velocity that the laminate can withstand without perforation.

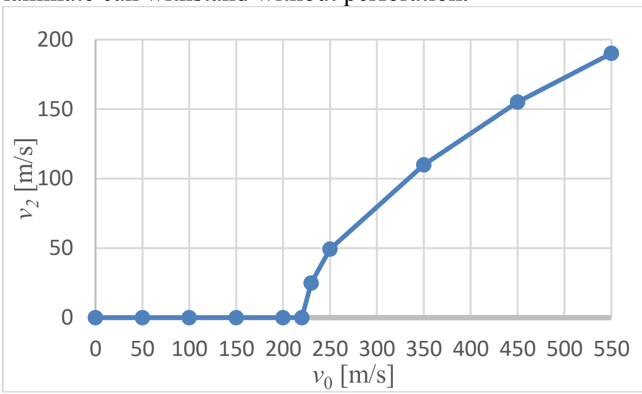

Fig. 11 *Ballistic limit of Kevlar 49 composite plate*

The obtained ballistic limit is not fully satisfactory, given that the actual projectile velocity may exceed this value. This indicates that the proposed design requires further improvement. Potential enhancements include increasing the impact resistance of the composite plate by enlarging its thickness or adding additional plies, as well as optimizing specific material and structural parameters to achieve a higher ballistic tolerance.

5 CONCLUSION

This study presented a procedure for evaluating the impact resistance of a composite plate, specifically examining its ability to absorb the kinetic energy of a projectile. Mathematical models were introduced, and the governing behavioral characteristics were identified. The analysis focused on a single configuration of the composite plate with fixed material properties, geometry, number and thickness of plies, and fiber orientations. The impactor, modeled as a 9 mm projectile, was also defined with precise material attributes and geometry. All of these factors represent constraints within the scope of the study, while the initial projectile velocity was the only parameter varied.
Future work may involve improving the performance of the proposed composite plate to achieve resistance to the entire range of velocities associated with a 9 mm projectile, as well as to impacts from other commercial ammunition, in accordance with relevant ballistic standards. Further optimization, such as adjusting selected design or material parameters, could enhance performance while simultaneously reducing the overall thickness and weight of the laminate. In [23], the optimization of a composite plate under low-velocity impact was conducted, suggesting the potential to extend the optimization algorithm to high-velocity impact scenarios. Additionally, the use of alternative materials with superior impact-resistant properties may provide further opportunities for advancement. Finally, modeling based on isogemetric FE approach [24] will be considered in the future work.
Experimental testing represents an essential component of the research process, serving to validate the mathematical models and numerical methods applied. Agreement between numerical and experimental results is crucial for confirming the reliability of the analyses, based on works cited [25, 26].

The presented methodology and findings may be applied in the development of protective equipment, such as ballistic vests and helmets, as well as in the design of lightweight and impact-resistant structures within the transportation industry.

REFERENCES

1. Huang, X., Su, S., Xu, Z., Miao, Q., Li, W., Wang, L., 2023, *Advanced Composite Materials for Structure Strengthening and Resilience Improvement*, Buildings,13(10), 240.
2. Schmidt, M., Pedersen, C.B., 2025, *Gradient-based optimization of CAD models addressing heterogeneous parameters and composite materials*, Structural and Multidisciplinary Optimization, 68(10), 209.
3. Tomasi, I., Grandi S., Solazzi, L., 2025, Implementation of Composite Materials for an Industrial Vehicle Component: A Design Approach, Journal of Composite Science, 9(4), 168.
4. Lin, Y., Qian, W., Lei, L., Liu, Y., Zhang, J., Liu, J., Kong, W., Hu, Y., Shi, Y., Wu, Z., Liu, H., Wu, S., 2025, *Structural integrity issues of composite materials and structures in future transportation equipment*, Composite Structures, 358, 118943.
5. Tserpes, K., Sioutis, I., 2025, *Advances in Composite Materials for Space Applications: A Comprehensive Literature Review*, Aerospace, 12(3), 215.
6. Kim, C., Lee, S., Rhee, K.Y., Park, S., 2024, *Carbon-based composites in biomedical applications: a comprehensive review of properties, applications, and future direction*, Advanced Composites and Hybrid Materials, 7, 55.
7. Monfared, M., Ramakrishna, S.,Alizadeh, A., Hekmatifar, M., 2023, *A systematic study on composite materials in civil engineering*, Ain Shams Engineering Journal, 14(12), 102251.
8. Setlak, L., Kowalik, R., Lusiak, T., 2021,*Practical Use of Composite Materials Used in Military Aircraft*, Materials, 14(17), 4812.
9. Devarajan, B., Lakshminarasimhan, R., Murugan, A., Rangappa, S.M., Siengchin, S., Marinkovic, D., 2024, *Recent developments in natural fiber hybrid composites for ballistic applications: a comprehensive review of mechanisms and failure criteria*, Facta Universitais Series Mechanical Engineering, 22(2), pp. 343-383.
10. Ma, D., Scazzosi, R., Manes, A., 2024,*Modeling approaches for ballistic simulations of composite materials: Analitical modes vs. finite element method*, Composites Science and Technology, 248, 110461.
11. Ha G.X., Marinkovic D., Zehn M.W., 2019, *Parametric investigations of mechanical properties of nap-core sandwich composites*, Composites Part B: Engineering, 161, pp. 427-438.
12. Guo, G., Alam, S., Peel, L., 2021, *An investigation of the effect of a Kevlar-29 composite cover layer on the penetration behavior of a ceramic armor system against 7.62mm APM2 projectiles*, International Journal of Impact Engineering, 157, 104000.
13. Tasić J., Marinković D., 2024, *FEM-Based Study of a Bullet Impact on a Composite Plate*, Innovative Mechanical Engineering, 3(1), pp. 79-89.
14. Yang, Y., Liu, Y., Xue, S., Sun, X., 2021,*Multi-scale finite element modeling of ballistic impact onto woven fabric involving fiber bundles*, Composite Structures, 267, 113856.
15. Meliande, N., Oliveira, M., Pereira, A., Balbino, F., Figuiredo, A., Monteiro, S.,Nascimento, L., 2023,*Ballistic properties of curaua-aramid laminated hybrid composites for military helmet*, Journal of Material Research and Technology, 25, pp. 3943-3956.
16. Akabi, T., Ansari, A., Pishbijari, M., 2023, *Influence of aluminium alloys on protection performance of metal matrix composite armor reinforced with ceramic particles under ballistic impact*, Ceramics International, 49(18), pp. 30937-30950.
17. Batra, R., Pydah. A., 2020, *Impact analysis of PEEK/ceramic/gelatin composite for finding behind armor trauma*, Composite Structures, 237, 111863.
18. Öztürk, E., Cavusoglu, O., Güral, A., 2025,*Experimental and Numerical Investigation of Strain Rate Dependent Flow and Fracture Behavior of 6181A-T4 Alloy Using the Johnson-Cook Model*, Crystals, 15(6), 528.
19. Sha, G.,Xiao, W., Lu, X., Zuo, H., Cao, M Ostachowicz, W.,2025, *Enhancing compressive failure prediction in repaired composites: A comparative study of 2D and 3D Hashin criteria with experimental validation*, Thin-Walled Structures, 217, Part B, 113911.
20. Soufri, A., Chettah, A., Bouvet, C., 2025,*Comparative Study of Composite Delamination Under Quasi-Simultaneous Impacts*, Aerospace, 12(8), 669.
21. Rama, G., Marinkovic, D., Zehn, M., 2018, *High performance 3-node shell element for linear and geometrically nonlinear analysis of composite laminates*, Composites Part B: Engineering, 151, pp. 118-126.
22. Rama, G., Marinkovic, D., 2016, *Efficient co-rotational 3-node shell element*, American Journal of Engineering and Applied Sciences, 9(2), pp. 420-431.
23. Tasić, J., Ćojbašić, Ž., Marinković, D., 2025, *Optimization of a Composite Plate Subjected to Low-Velocity Impact*, Applied Science, 15(21), 11659.
24. Milić, P., Marinković, D., Klinge, S., Ćojbašić, Ž., 2023, *Reissner-Mindlin Based Isogeometric Finite Element Formulation for Piezoelectric Active Laminated Shells*, Tehnički Vjesnik, 30(2), pp. 416-425.
25. Zachariah, A.S., Shenoy, S., Pai, D., 2024, *Experimental Analysis of the Effect of the Wowen Aramid Fabric on the Strain to Failure Behavior of Plain Weaved Carbon/Aramid Hybrid Laminates*, Facta Universitatis Series Mechanical Engineering, 22(1), pp. 13-24.
26. Gawryluk, J., Teter, A., 2021, *Experimental-numerical studies on the first-ply failure analysis of real, thin walled laminated angle columns subjected to uniform shortening*, Composite Structures, 269(8), 114046.

Contact address:
Jovica Tasić
University of Niš
Faculty of Mechanical engineering
18000 Niš
A. Medvedeva 14
E-mail: jovicatsc93@gmail.com